Surface electronic properties of d-band perovskites: Study of the π bands

Ş. Ellialtioğlu* and T. Wolfram
Department of Physics, University of Missouri-Columbia, Columbia, Missouri 65201
(Received 30 August 1976)

The surface electronic properties of d-band perovskites such as $SrTiO_3$ are investigated in some detail using a Green's-function method and a linear-combination-of-atomic-orbitals model developed in our previous work. We consider the nine energy bands (π bands) associated with the t_{2g} d orbitals of the cation and the corresponding p orbitals of the oxygen ions. Exact expressions for the local density of states (LDS) of cations and anions at and near a (001) surface are derived and evaluated for a variety of surface conditions. It is found that the LDS of a surface cation is substantially enhanced in the energy range of the filled valence bands when surface states occur in the forbidden band gap. This increase in density results from surface enhancement of the covalent mixing of d orbitals into valence-band wave functions. The surface-enhanced covalency leads to a substantial increase in the number of electrons occupying surface cation d orbitals if intra-atomic Coulomb repulsion is neglected. An approximate Hartree-Fock treatment is employed to investigate the effect of Coulomb repulsion among excess electrons in surface orbitals. Approximately self-consistent solutions for the LDS are obtained. These solutions show that band-gap surface states are forced to lie substantially nearer to the conduction-band edge than predicted by the non-self-consistent theory. Two competing effects arise when the electron occupation is altered on the surface cations. First, there is an increase in the interatomic Coulomb repulsion among the excess d-orbital electrons. Second, there is a corresponding decrease in the interatomic Coulomb repulsion (Madelung potentials) because of the reduction in the ionic charges. The intra-atomic Coulomb repulsion dominates for the case of an ideal surface and surface bands are repelled from the midgap region. It is suggested that a surface oxygen vacancy concentration of a few percent can alter the balance between interatomic and intra-atomic Coulomb repulsion resulting in the appearance of band-gap surface bands. These results are employed to suggest a possible explanation of the results of several recent photoemission experiments on the surface states of $SrTiO_3$ and TiO_2.

I. INTRODUCTION

A. Background

The transition-metal oxides are of current interest because of their catalytic[1] and electrocatalytic[2,3] properties. These properties are presumed to be associated with the localized states of the surface cations, anions, and oxygen vacancies. A detailed first-principles determination of the nature of these surface states is not yet available.

Many of the transition-metal oxides are ionic and have a common local structure approximated by a positively charged cation at the center of an octahedron of negatively charged oxygen anions. The dominant features of this structure are bonding and antibonding wave functions that are admixtures of oxygen p orbitals and cation d orbitals. In the solid, these states may be broadened into valence and conduction energy bands or when the electron correlation is large they may retain the properties of localized "crystal-field states."

The cubic perovskites are a class of the transition-metal oxides having the formula unit ABO_3, where B represents the transition-metal ion. Many of the perovskites such as $SrTiO_3$, $BaTiO_3$, $KMoO_3$, ReO_3, and a large number of others have (delocalized) band states. We refer to these solids possessing conventional energy bands as "d-band perovskites." This work is concerned with the surface electronic structure of the d-band perovskites.

In previous papers[4] we developed a simple exactly solvable linear-combination-of-atomic-orbitals (LCAO) model which produces a good description of the electronic properties of d-band perovskites. Using this model we obtained simple analytic expressions for the energy bands, wave functions,[4] d-band density of states, the frequency-dependent dielectric function and optical reflectivity.[5] The energy bands and density of states were shown to be in good agreement with the augmented-plane-wave calculations of Mattheiss.[6] The structures in the dielectric function and optical reflectivity predicted by the model were found to be in excellent agreement with the experimental measurements of Cardona[7] for $SrTiO_3$ and $BaTiO_3$.

Because of the success of the model in representing many of the bulk properties, we were encouraged that it would also serve as a useful model for studying surface states and chemisorption on the d-band perovskites. Analytical calculations of the surface energy bands for a (001) surface were reported in previous papers.[4,8]

Two types of (001) surfaces are possible for the perovskites. The type-I surface has the transition-

metal ion exposed on the surface while for the type-II surface they are covered with a layer of oxygen ions. Our calculations indicated that a surface-state band derived from the lower conduction band (π^* band) could occur in the band gap between the π^* band and the upper valence band (π band).

The position of the surface band depends upon parameters which characterize the surface. For an ideal type-I (001) surface the Madelung potential at a surface cation is less repulsive than at an interior site.[9] This surface perturbation produces a surface energy band which extends in energy from about the center of the band gap to the edge of the π^* band.[4] The corresponding surface states were also found in our studies[10] of TiO_6 and TiO_5 clusters.

The d-electron surface states of the π^* band are of particular interest because they possess the proper symmetry for strong interaction with the valence states of many different molecules.[11]

Recent photoemission experiments on surfaces of reduced $SrTiO_3$ by Powell and Spicer,[12] and on TiO_2 and $SrTiO_3$ by Henrich, Dresselhaus, and Zeiger[13] may be summarized as follows: (i) cleaved (or fractured) surfaces of TiO_2 or $SrTiO_3$ do not have surface states in the band gap; (ii) well-ordered $SrTiO_3$ surfaces that have been cut, polished, etched, and annealed in vacuum do possess band-gap surface states, but similarly prepared TiO_2 surfaces show no band-gap states; (iii) band-gap surface states appear for both TiO_2 and $SrTiO_3$ when the surfaces are bombarded with Ar^+ ions; (iv) exposure to oxygen removes the band-gap states; and (v) low-energy-electron-diffraction (LEED) patterns indicate that cleaved or fractured surfaces of $SrTiO_3$ or TiO_2 are more disordered than surfaces annealed in vacuum.

These surface properties are not well understood but it is believed that the concentration of surface oxygen vacancies plays a vital role in stabilizing the band-gap states. Henrich *et al.*[13] have discussed these phenomena from the point of view of localized states associated with isolated Ti^{3+} surface ions charge compensated by oxygen vacancies. In this paper, we develop further the energy band description which should be valid for well-ordered surfaces with modest concentrations of oxygen vacancies.

In this work, we consider the changes in the electron occupation of surface d-orbital due to the presence of a surface. We study the effect of changes in the Coulomb repulsion among d electrons on the behavior of the surface energy bands of perovskites. We calculate the local density of states associated with d electrons on cations and p electrons on oxygen ions at and near a (001) surface. We find that the electron occupation of surface cation d orbitals is substantially increased from that of interior cations. This increase in electrons on surface cations results from increased covalent mixing of the p and d orbitals which make up the filled valence bands of the *finite* crystal. Owing to this "surface enhanced covalency" the effect of Coulomb repulsion among d electrons is large even if the band-gap surface states are unoccupied.

When Coulomb repulsion is considered, the surface states must be determined self-consistently. We assume as a starting point an LCAO model representing a self-consistent description of the energy bands of the infinite or bulk crystal. We then treat self-consistently the Coulomb repulsion due to changes in the d-orbital electron occupation due to the presence of the surface. We find that there is a competition between the electrostatic Madelung potential and the Coulomb energy. Additional electrons added to surface cations come from the oxygen anions. This reduces the formal ionic charges of both species which in turn reduces the magnitude of the Madelung potentials. Reduction of the Madelung potential at a surface-cation site tends to drop cation surface bands into the band-gap region. On the other hand the repulsion among excess d electrons tends to raise the surface state out of the band gap towards the conduction-band region. When the Coulomb energy dominates the Madelung energy, self-consistent surface energy bands tend to be forced away from the midgap region. As the Fermi level is raised (by reduction of the sample for example), the surface bands tend to rise with the Fermi level so that their occupation is small. Thus, in contrast to simple semiconductors where the surface states pin the Fermi level, it appears as though the Fermi level pins the surface states.

The presence of surface oxygen vacancies can substantially alter these conclusions about the position of the surface band. Each surface vacancy contributes an attractive contribution of 7 to 10 eV to the Madelung potential at the six near- and next-nearest-neighbor cation sites. A modest concentration of surface vacancies can alter the balance between intra-atomic Coulomb energy and interatomic Coulomb energy causing the Madelung potential change to dominate. In such a case, the band-gap surface states are stabilized by the vacancies.

B. Model for surface properties

In this work, we use our LCAO model for the t_{2g} or π bands of d-band perovskites to study the LDS (local density of states) of cations and anions at and near a (001) surface.

In Sec. II, we describe the model Hamiltonian for a d-band perovskite with a (001) surface including nearest-neighbor cation-anion interactions and the effects of variations in the surface Madelung potentials. The change in Coulomb repulsion energy associated with changes in the electron occupation of d orbitals is treated in the Hartree-Fock approximation.

In Sec. III, we use a lattice-space Green's-function method to obtain solutions for the cation and anion local-density-of-states (LDS) functions. The general features of the bulk and surface states are described. In Sec. IV, we present explicit results for the LDS functions and their dependence on the model parameters. The effects of electron-electron interactions of the d electrons are included in an approximate way. In Sec. V, we give a discussion of how the results may relate to the recent photoemission and electron energy loss experiments. Finally, we present in the Appendices, detailed discussions of the mathematical properties of the various Green's functions involved in the LDS functions.

II. MODEL HAMILTONIAN FOR d-BAND PEROVSKITES

The qualitative features of the electronic states of the d-band perovskites have been reviewed in detail in our previous work[4,5,8] and elsewhere.[14] The ABO_3 structure and the Brillouin zone are illustrated in Figs. 1 and 2. The energy bands derived from the cation d orbitals and the anion p orbitals are of principle interest. The bands derived from $4s$ and $4p$ cation states are located approximately 10 eV above the band gap and the bands associated with the $2s$ oxygen states are equally far below the band gap. For this reason we neglect these bands in our model. In the ABO_3 perovskites the A ion produces energy bands which are also far removed from the band gap and do not play an important role in determining the electronic properties. Thus, the only important effect of the A ion is its electrostatic contribution to the Madelung potentials and the crystalline field.

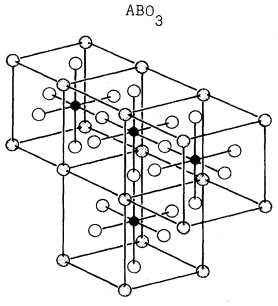

FIG. 1. ABO_3 cubic perovskite structure. The solid circles represent the B or transition-metal ions, the open circles are the oxygen ions and the shaded circles are the A ions.

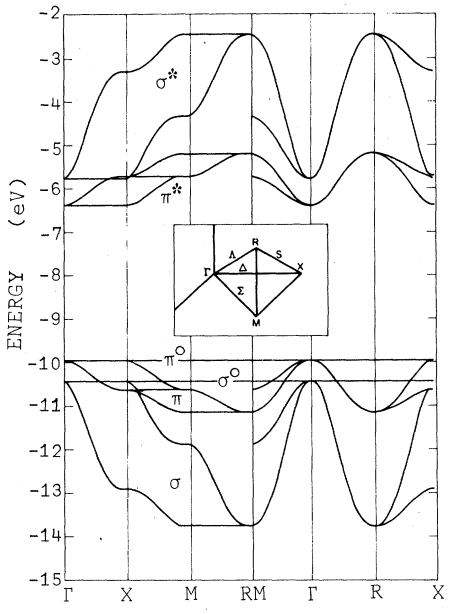

FIG. 2. Energy bands of $SrTiO_3$ according to the nearest-neighbor LCAO model (Ref. 4), with $E_t = -6.3$, $E_\pi = -10.0$, $pd\pi = 0.84$, and $pd\sigma = 2.1$ eV. The symmetry points in the first Brillouin zone for the cubic perovskite structure ABO_3 are shown in the center.

Therefore, within these approximations the properties of the perovskites are determined by the BO_3 part of the ABO_3 structure. In this respect, the pseudoperovskite ReO_3 is a regular member of the family of oxides that we shall investigate.

The Hamiltonian for the oxide is as follows:

$$H = H_d + H_p + H_{pd}\,, \tag{2.1}$$

$$H_d = \sum_{R_d,\alpha} E_d(R_d,\alpha)\, n_d(R_d,\alpha)\,, \tag{2.2}$$

$$H_p = \sum_{R_p,\beta} E_p(R_p,\beta)\, n_p(R_p,\beta)\,, \tag{2.3}$$

$$H_{pd} = \sum_{R_d,\alpha} \sum_{R_p,\beta} [T_{\alpha\beta}(R_d,R_p)\, d^\dagger_\alpha(R_d)\, p_\beta(R_p) + \text{H.c.}]\,, \tag{2.4}$$

$$n_d(R_d,\alpha) = d^\dagger_\alpha(R_d)\, d_\alpha(R_d)\,, \qquad n_p(R_p,\beta) = p^\dagger_\beta(R_p)\, p_\beta(R_p)\,. \tag{2.5}$$

In Eq. (2.5), $n_d(R_d,\alpha)$ is the number operator for d orbitals and $d^\dagger_\alpha(R_d)$ is an operator which adds an electron to a d-orbital-of-symmetry type α located on a cation site at R_d. The operator $p^\dagger_\beta(R_p)$ adds an electron to a p-orbital-of-symmetry type β ($\beta = x$, y, or z) on an anion site at R_p and $n_p(R_p,\beta)$ is the corresponding number operator. We assume orthogonalized orbitals so that the operators obey the usual commutation relations.

In Eq. (2.2), $E_d(R_d,\alpha)$ is the effective diagonal energy of an electron occupying a cation d orbital located at the lattice position R_d. The symbol α designates the symmetry type, $\alpha = xy$, xz, yz, $3z^2-r^2$, or x^2-y^2. $E_d(R_d,\alpha)$ includes the effects of the Madelung potentials and electrostatic contribution to the crystal field. We also include in $E_d(R_d,\alpha)$ a simple Hartree-Fock approximation to the Coulomb repulsion among electrons occupying d orbitals centered on the same site. We write

$$E_d(R_d,\alpha) = E_d^0(\infty,\alpha) + U_d\langle\Delta n_d(R_d)\rangle + \Delta V_{es}(R_d), \tag{2.6}$$

where $E_d^0(\infty,\alpha)$ is the effective energy of the d orbital for an infinite crystal including electrostatic and correlation effects and the remaining terms are associated with the presence of a surface. The second term of Eq. (2.6) represents the change in the Coulomb repulsion among electrons on a d orbital at R_d due to surface induced changes in the d-orbital occupancy. The quantity $\langle\Delta n_d(R_d)\rangle$ is the change in the total d-orbital occupancy including all symmetry types, and U_d is the effective Coulomb integral. The third term in Eq. (2.6) accounts for changes in the Madelung potential and crystal field due to the surface.

It has been previously shown that on a type-I surface the Madelung potential at a surface cation site is less repulsive than at an interior site[9] assuming that $\langle\Delta n_d(R_d)\rangle = 0$. If $\langle n_d(R_d)\rangle$ varies at or near the surface there will be two competing effects. First, an increase in $\langle n_d(R_d)\rangle$ will introduce additional Coulomb repulsion which reduces the effective ionization energy $E_d(R_d,\alpha)$. On the other hand, because of charge neutrality an increase in $\langle n_d(R_d)\rangle$ must be accompanied by a corresponding decrease in charge on the oxygen ions. Therefore the formal charges on both cations and anions will be reduced when $\langle n_d(R_d)\rangle$ increases. As a result, the repulsive Madelung potential at cation site will be reduced leading to an increase in the effective ionization energy.

Changes in d-orbital occupation can occur because of the redistribution of the LDS associated with highly localized surface states. For simplicity and to a good approximation we can assume that $\langle\Delta n_d(R_d)\rangle$ is nonvanishing only when R_d designates a surface site and that changes in ionic charges are limited to the surface unit cell. Then, since charge neutrality imposes a proportionality between anion and cation charges we are able to write the change in the Madelung potential at the surface cation site approximately as

$$\Delta V_M(R_s) \simeq -\Delta V_M^0 - C_M\langle\Delta n_d(R_s)\rangle, \tag{2.7}$$

where R_s designates a surface site, $-\Delta V_M^0$ is the change when $\langle\Delta n_d(R_s)\rangle = 0$, and C_M is a constant to be discussed later.

In addition to the Madelung contribution to ΔV_{es} there is also a change in the electrostatic crystal field. Cations at the surface will experience an axial-field component which introduces additional splitting. We assume that the covalent contribution to the axial field dominates and neglects the electrostatic axial-field contribution.

In summary, we have

$$E_d(R_d,\alpha) \simeq E_d^0(\infty,\alpha) + [-\Delta V_M^0 + (U_d - C_M)\langle\Delta n_d(R_d)\rangle]\,\delta_{R_d,R_s}. \tag{2.8}$$

The effective-ionization energy for a p orbital $E_p(R_p,\beta)$ includes electrostatic, crystal field, and correlation effects. An increase in Δn_d implies a decrease in Δn_p and therefore, the anion effective-ionization energy is increased with increasing Δn_d. The stabilizing attractive Madelung potential, however, is reduced. A decomposition analogous to that of Eq. (2.8) should be considered for the oxygen ions in the surface unit cell. For a type-I surface ΔV_M^0 at the oxygen site is known to vanish approximately.[9] Because there are three oxygen ions per unit cell, the change in anion charge is much smaller than that of the cation and the Coulomb integral is also smaller. There is also approximate cancellation between the Madelung and correlation energies, and therefore, for simplicity we shall neglect spatial variations in $E_p(R_p,\beta)$. This approximation is not essential in what follows but it greatly simplifies the theory.

The interaction between cations and anions is expressed by Eq. (2.4). The quantities $T_{\alpha\beta}(R_p,R_d)$ are LCAO transfer integrals. For nearest-neighbor interactions only the transfer integrals $pd\pi$ and $pd\sigma$ are required. The nature of these interactions has been previously discussed by many authors.[5,6,14,15]

A. Properties of the infinite solid

Before describing the solutions for the finite solid we first discuss the properties of the infinite solid.

Using the Hamiltonian described by Eqs. (2.1)–(2.5) with $\langle\Delta n_d\rangle = 0$, one can easily find expressions for the bulk energy bands. The model involves 14 basis states: five d orbitals and nine p orbitals (three for each of the three oxygen ions in a unit cell). Therefore there are 14 energy bands. These bands are illustrated in Fig. 2 for values of the LCAO parameters representative of $SrTiO_3$.[4]

The energy bands may be understood as consisting of a set of three equivalent π^* conduction and π

valence bands. The wave functions for these bands are admixtures of t_{2g}-symmetry (xy, xz, and yz) d orbitals with p orbitals whose lobes are oriented perpendicular to the B-O axis; (p_π states). These orbitals are admixed through the LCAO interaction parameter $pd\pi$ and the energy of the bands are given by

$$E_{\alpha\beta} = \tfrac{1}{2}(E_t + E_\pi) \pm \{[\tfrac{1}{2}(E_t - E_\pi)]^2 + 4(pd\pi)^2 (S_\alpha^2 + S_\beta^2)\}^{1/2},$$
$$\alpha\beta = xy,\ xz,\ \text{or}\ yz, \qquad (2.9)$$
$$S_\alpha = \sin(k_\alpha a).$$

In Eq. (2.9), E_t and E_π are the diagonal energies of the t_{2g} and p_π orbitals including the Madelung potentials, electrostatic crystal-field splitting and the effect of Coulomb repulsion. The quantity $pd\pi$ is the LCAO transfer integral and k_α is the αth Cartesian component of the energy band wave vector. These bands are referred to as the π bands. In analogy with molecular bonding and antibonding notation, the conduction band is designated as the π^* band (antibonding) while the valence band is referred to as the π band (bonding). The π bands are the upper valence band and the lower conduction band as shown in Fig. 2. (In previous work we have referred to the π^* band as the t_{2g} band.)

A second set of bands are formed from the admixtures of the e_g cation orbitals (x^2-y^2, and $3z^2-r^2$) with p orbitals having their lobes oriented parallel to the B-O axis (p_σ states). The energy of these four so-called σ bands is given by

$$E_{xyz} = \tfrac{1}{2}(E_e + E_\sigma) \pm \{[\tfrac{1}{2}(E_e - E_\sigma)]^2 + 2(pd\sigma)^2 (S_x^2 + S_y^2 + S_z^2 \pm S^2)\}^{1/2},$$

with

$$S^4 = S_x^4 + S_y^4 + S_z^4 - S_x^2 S_y^2 - S_x^2 S_z^2 - S_y^2 S_z^2. \qquad (2.10)$$

where E_e and E_σ are defined in a manner analogous to E_t and E_π, $pd\sigma$ is the corresponding LCAO transfer integral, and the + (−) corresponds to the σ^* (σ) band.

In addition to the π and σ bands just described, there are two nonbonding bands. One of these bands involves p_π orbitals and no admixture with cation orbitals. This π-nonbonding band is triply degenerate. We shall designate these nonbonding states by π^0. The other, namely, the σ^0 band, involves only p_σ orbitals, and is nondegenerate. These bands have energies given by

$$E(\pi^0\ \text{band}) = E_\pi, \quad E(\sigma^0\ \text{band}) = E_\sigma.$$

In Fig. 3, we compare the energy bands of the simple model (dashed curves) with a full LCAO model fit to the augmented-plane-wave results of Mattheiss[6] for $SrTiO_3$. It is evident that the model

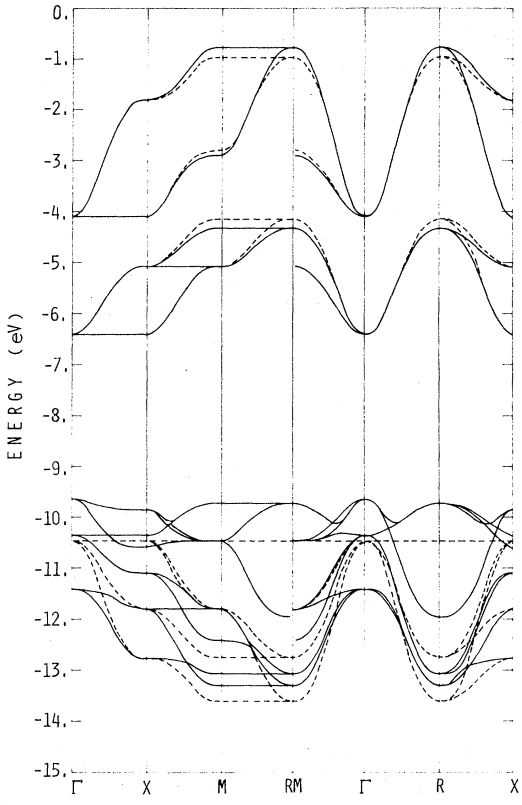

FIG. 3. Comparison of energy bands obtained from the nearest-neighbor LCAO model using the parameters $E_t = -6.4$, $E_\pi = -10.5$, $pd\pi = 1.34$ and $pd\sigma = -2.23$ eV (dashed curves), and those of the full LCAO model fit to APW results of Mattheiss (Ref. 6) with $pp\sigma = 0.34$ and $pp\pi = -0.03$ eV (solid curves).

gives an excellent fit to the d bands. To illustrate how well the model represents these bands, we show, in Fig. 4, a comparison of the theoretical π^*-band density of states with the numerical results of Mattheiss. The theoretical curve shown is the density of states of the π^*-band given by

$$\rho_{\pi^*}(E) = \frac{1}{\pi^2} \frac{|E - \tfrac{1}{2}(E_t + E_\pi)| K(\xi')}{(pd\pi)^2}, \qquad (2.11)$$

with

$$\xi^2 = (\epsilon/4)^2, \quad \xi' = (1 - \xi^2)^{1/2}$$
$$\epsilon = [(E - E_t)(E - E_\pi) - 4(pd\pi)^2]/(pd\pi)^2.$$

where $K(\xi^{-1})$ is the complete elliptic integral of the first kind with modulus ξ^{-1}. (The derivation of this result is described in Sec. III.)

The valence bands given by the model differ from the solid curves in Fig. 3 principally in the behavior of the nonbonding bands. The simple model yields "flat" bands while the actual bands have some dispersion. The origin of the dispersion is

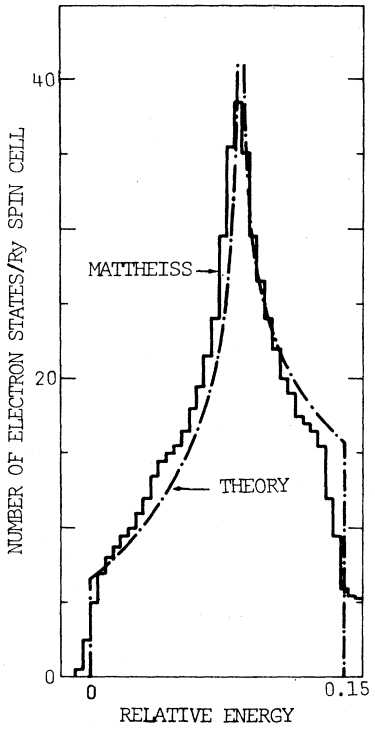

FIG. 4. Comparison of densities of states of the π^* bands of $SrTiO_3$ as calculated from the model in this paper (theory) and as determined by Mattheiss (Ref. 6). For the curve shown, $pd\pi = 1.34$ eV.

the anion-anion transfer integrals which are neglected in our simple model since they are second-neighbor interactions.

It is noted from Eq. (2.9) that each of the π bands is two dimensional in the sense that each band depends only on two components of the three-dimensional k vector. This two-dimensional character[5] is responsible for the jump discontinuities at the π-band edge and the logarithmic singularity at the band center seen in the π^*-band density of states in Fig. 4. The origin of these two-dimensional bands is the planar character of the $pd\pi$ interaction. It is easily verified that each π band involves only the $\alpha\beta$ d orbital and the α and β p orbitals. For example the wave functions for E_{xy} are linear combinations of d_{xy}, p_x, and p_y.

The remainder of this paper will be devoted to a study of the surface electronic structure associated with the π bands of the perovskites.

III. LATTICE GREEN'S FUNCTIONS

A. Definitions

Our objective is to calculate the LDS of cations and anions at or near the surface of a semi-infinite d-band perovskite with a (001) type-I surface. To do this we need to calculate the matrix elements of the lattice-space Green's functions.

We make use of the retarded Green's functions defined by

$$G_{\alpha\alpha'}(R,R';t) \equiv -i\Theta(t)\langle [C_\alpha(R,t), C^\dagger_{\alpha'}(R',0)]_+ \rangle . \tag{3.1}$$

The properties of these functions have been described in detail elsewhere.[16] In Eq. (3.1), $\Theta(t)$ is a step function equal to unity for $t>0$, and zero otherwise. The operator $C_\alpha(R,t)$ or $C^\dagger_{\alpha'}(R',0)$ designate any one of the operators d_α and p_β appearing in the model Hamiltonian. Each combination gives a matrix element of the lattice-space Green's-function matrix.

We define the energy-dependent Green's-function matrix elements by

$$G_{\alpha\alpha'}(R,R';E) = \int_{-\infty}^{+\infty} dt\, e^{iEt} G_{\alpha\alpha'}(R,R';t) . \tag{3.2}$$

The LDS for a cation at R_d or an anion at R_p is given by

$$\rho_\alpha(R) = (-1/\pi)\mathrm{Im}G_{\alpha\alpha}(R,R;E) . \tag{3.3}$$

B. Calculation of $G_{\alpha\alpha'}$ for the π bands

We restrict our attention to the π bands and consider the situations illustrated schematically in Fig. 5. The sets of orbitals [shown in Fig. 5(a)] $\{d_{xz}, p_x^{(1)}, p_z^{(2)}\}$, $\{d_{xy}, p_y^{(2)}, p_x^{(3)}\}$ and $\{d_{yz}, p_y^{(1)}, p_z^{(3)}\}$ are uncoupled orthogonal sets of basis orbitals which produce the three equivalent π bands in the infinite solid. These sets remain uncoupled for the semi-infinite solid with a (001) surface but they are no longer equivalent. For the semi-infinite solid, xz is equivalent to yz, but xy is different.

The problem of calculating the π states of the semi-infinite solid reduces to the solution of two uncoupled systems as illustrated in Figs. 5(b) and 5(c).

First consider the problem represented by Fig. 5(b). We locate a cation or anion by specifying n and l which locate a unit cell relative to the surface and to the $l=0$ origin. The (n,l) designation together with the symmetry index uniquely specifies the orbital and its location. In this notation,

$$G_{\alpha,\alpha'}(R,R';E) \rightarrow G_{\alpha,\alpha'}(n,l;n',l') .$$

Using standard methods to generate the equations of motion we obtain

$$[\omega-\epsilon_t(n)]G_{xz,\gamma}(n,l;n',l')=\delta_{xz,\gamma}\delta_{n,n'}\delta_{l,l'}+G_{x,\gamma}(n,l;n',l')$$
$$-G_{x,\gamma}(n-1,l;n',l')(1-\delta_{n,0})+G_{z,\gamma}(n,l;n',l')-G_{z,\gamma}(n,l-1;n',l')\,, \quad (3.4)$$

$$[\omega-\epsilon_x(n)]G_{x,\gamma}(n,l;n',l')=\delta_{x,\gamma}\delta_{n,n'}\delta_{l,l'}+G_{xz,\gamma}(n,l;n',l')-G_{xz,\gamma}(n+1,l;n',l')\,, \quad (3.5)$$

$$[\omega-\epsilon_z(n)]G_{z,\gamma}(n,l;n',l')=\delta_{z,\gamma}\delta_{n,n'}\delta_{l,l'}+G_{xz,\gamma}(n,l;n',l')-G_{xz,\gamma}(n,l+1;n',l')\,, \quad (3.6)$$

where $\gamma=xz$, x, or z. In Eqs. (3.4)–(3.6), we have introduced the dimensionless parameters

$$\epsilon_t(n)=\frac{E_t^0+[-\Delta V_M^0+(U_d-C_M)\langle\Delta n_d(0)\rangle]\delta_{n,0}}{pd\pi}\,, \quad (3.7)$$

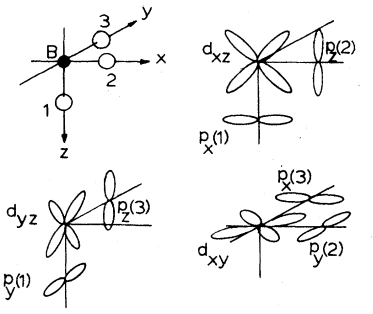

(a)

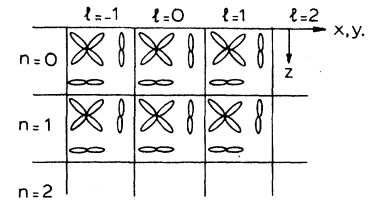

(b)

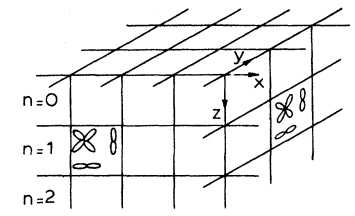

(c)

FIG. 5. Schematic of the geometry and orbitals involved in calculation of π bands on a (001) perovskite surface. (a) Unit cell for the BO_3 structure and the three equivalent sets of orbitals. (b) The squares indicate the two-dimensional unit cells each of which contains one cation and two anion orbitals. The position of an ion is designated by n, the number of unit cells from the surface, and l, the number of unit cells from the $l=0$ cell. (c) Three-dimensional picture with a (001) surface.

$$\epsilon_x(n)=\epsilon_y(n)=\epsilon_\pi=\frac{E_\pi}{pd\pi}\,,\quad \omega=\frac{E}{pd\pi}\,, \quad (3.8)$$

where E_t and E_π are the infinite solid values for the diagonal matrix elements including U_d or U_p and the bulk Madelung potentials. The changes in occupations are given by

$$\Delta n_d(n)=\sum_{(d\alpha)}\langle n_d(n,d\alpha)-n_d(\infty,d\alpha)\rangle\,, \quad (3.9)$$

$$n_d(n,d\alpha)=\int_{-\infty}^{\epsilon_F}d\omega\,\rho_{(d\alpha)}(n)\,. \quad (3.10)$$

In Eq. (3.9) and (3.10), the notation $(d\alpha)$ designates the various d-symmetry orbitals and $\rho_\gamma(n)$ is defined by Eq. (3.3). The quantity $n_d(\infty)$ is the occupation number for the infinite solid (no surface) or for a site very distant from the surface.

The system of Eqs. (3.4)–(3.6) are easily solved using the method employed in our previous paper.[4] The following results are obtained for the Green's-function matrix elements:

$$G_{xz,xz}(n,l;n',l')$$
$$=(\omega-\epsilon_\pi)[\mathcal{G}(n+n',l-l')-g_\epsilon(n+n',l-l')$$
$$+g_\epsilon(|n-n'|;l-l')]\,. \quad (3.11)$$

The functions $\mathcal{G}(n,l)$ and $g_\epsilon(n,l)$ are defined by

$$\mathcal{G}(n,l)=\frac{1}{\pi}\int_0^\pi dK\frac{e^{in\theta(\omega,K)}e^{ilK}}{\Delta p(\omega)-e^{-i\theta(\omega,K)}}\,, \quad (3.12)$$

$$g_\epsilon(n,l)=\frac{1}{2\pi i}\int_0^\pi dK\,\frac{e^{in\theta(\omega,K)}e^{ilK}}{\sin\theta(\omega,K)}\,, \quad (3.13)$$

and

$$\Delta p(\omega)=1-(\omega-\epsilon_\pi)\Delta\epsilon_t\,, \quad (3.14)$$

$$\Delta\epsilon_t=[-\Delta V_M^0+(U_d-C_M)\Delta n_d(0)]/pd\pi\,, \quad (3.15)$$

with the function $\theta(\omega,K)$ defined through relations

$$-2\cos\theta(\omega,K)=2\cos K+\epsilon\,, \quad (3.16)$$

$$\epsilon=(\omega-\epsilon_\pi)(\omega-\epsilon_t)-4\,. \quad (3.17)$$

These functions can be evaluated exactly in terms of elliptic integrals of the first, second, and third kind. [Evaluation of the functions $\mathcal{G}(0,0)$ and $g(0,0)$ which are required in this paper is described in the Appendices.] The Green's function for a surface cation obtained from Eq. (3.11) with $n=n'=0$ and $l=l'$ is

$$G_{xz,xz}(0,0,l,l) \equiv G_{xz}(0) = (\omega - \epsilon_\pi)\, \mathcal{G}(0,0)\,. \tag{3.18}$$

Then using Eq. (3.4)–(3.6) together with Eq. (3.18) we obtain

$$G_{z,z}(0,0,l,l) \equiv G_z(0) = (\omega - \epsilon_\pi)^{-1}[(2+\epsilon+\Delta p)\mathcal{G}(0,0) + \mathcal{G}(1,0)]\,, \tag{3.19}$$

$$G_{x,x}(0,0,l,l) \equiv G_x(0) = (\omega - \epsilon_\pi)^{-1}[1 + 2\mathcal{G}(0,0) - (2+\Delta p)\mathcal{G}(1,0) + \mathcal{G}(2,0)]\,. \tag{3.20}$$

It is convenient to work with the sum $G_x(0) + G_z(0)$ since from Eqs. (3.14), (3.17), (3.19), and (3.20),

$$G_x(0) + G_z(0) = (\omega - \epsilon_t - \Delta\epsilon_t)\mathcal{G}(0,0) + (\omega - \epsilon_\pi)^{-1}[1 + \mathcal{G}(0,0) - (1+\Delta p)\mathcal{G}(1,0) + \mathcal{G}(2,0)]\,. \tag{3.21}$$

Returning to Eq. (3.11) and using the fact that $|\mathcal{G}(n,l)|$ and $|g(n,l)|$ tend to zero exponentially for large n we see that in the interior, far from the surface

$$\lim_{n\to\infty} G_{xz,xz}(n,n,l,l) \equiv G_{xz}(\infty) \to (\omega - \epsilon_\pi) g_\epsilon(0,0) \tag{3.22}$$

and

$$[G_x(\infty) + G_z(\infty)] \to 1/(\omega - \epsilon_\pi) + (\omega - \epsilon_t) g_\epsilon(0,0)\,. \tag{3.23}$$

C. Properties of $G_\alpha(\infty)$

The function of $g_\epsilon(0,0)$ is a Green's-function characteristic of the infinite solid. In Appendix A we show that

$$g_\epsilon(0,0) = \begin{cases} (1/2\pi)(1/\xi)K(1/\xi) & \text{for } (\tfrac{1}{4}\epsilon)^2 > 1\,, \\ (1/2\pi)[\mathrm{sgn}(\xi)K(\xi) - iK(\xi')] & \text{for } (\tfrac{1}{4}\epsilon)^2 \le 1\,, \end{cases} \tag{3.24, 3.25}$$

with

$$\xi = \tfrac{1}{4}\epsilon, \quad \xi' = (1-\xi^2)^{1/2}.$$

The result of Eq. (3.23) is the anion Green's function for the infinite solid. The term $(\omega - \epsilon_\pi)^{-1}$ is the contribution due to π^0 band. This term produces a δ function contribution to the density of states at $\omega = \epsilon_\pi$. The second term contributes a density of states to the π bands (both the π^* and π bands). Adding this term to the imaginary part of $G_{xz}(\infty)$ gives the total density of π-band states

$$\rho_\pi(\omega) = (1/2\pi^2)\,|\,2\omega - \epsilon_\pi - \epsilon_t\,|\,K(\xi')\,. \tag{3.26}$$

Equation (3.26) is equivalent to the result given by Eq. (2.11) in Sec. II.

D. Properties of $\mathcal{G}(0,0)$

From Eq. (3.12) we have for $n = l = 0$,

$$\mathcal{G}(0,0) = \frac{1}{\pi}\int_0^\pi \frac{dK}{\Delta p(\omega) - e^{-i\theta(\omega,K)}}\,. \tag{3.27}$$

This function is a Green's-function characteristic of the semi-infinite solid. Analytic expressions for $\mathcal{G}(0,0)$ are given in Appendix B. The general properties are evident from Eq. (3.27). The quantity $e^{-i\theta}$ is defined through the relations of Eqs. (3.16) and (3.17). The function $\theta(\omega,K)$ is real for values of (ω,K) which lie within the π bands described by Eq. (2.9). For such values of (ω,K), the function $e^{-i\theta}$ is complex and consequently $\mathcal{G}(0,0)$ will possess an imaginary part. The imaginary part of $(\omega - \epsilon_\pi)\,\mathcal{G}(0,0)$ in this range is the cation LDS which lies within the π bands of the bulk solid. Since $e^{-i\theta}$ is complex, the denominator of the integrand in Eq. (3.27) cannot vanish and the density arises from branch cut contributions.

For (ω,K) outside of the π bands or within the band gap, $e^{-i\theta}$ is real. The denominator of the integrand will vanish when

$$\Delta p(\omega) = e^{-i\theta(\omega,K)}$$

which is the surface-state condition, or

$$\Omega \equiv \frac{\Delta p^2(\omega) + 1}{2\Delta p(\omega)} + \frac{\epsilon(\omega)}{2} = -\cos K\,. \tag{3.28}$$

In our previous paper,[4] we showed that if Eq. (3.28) is satisfied then a surface state can exist. The surface energy bands are determined by finding the values of ω and K which satisfy Eq. (3.28). In general, more than one surface band can occur and the bands need not exist for all values of K in the surface Brillouin zone.

Thus for a fixed value of ω, the denominator of the integrand of $\mathcal{G}(0,0)$ will vanish for some value of K if a surface state exists for that value of ω. This produces a simple-pole contribution to the LDS.

In summary, the imaginary part of $\mathcal{G}(0,0)$ arises from two sources. The first is due to branch-cut contributions associated with bulklike states in the π bands, and the second is due to pole contributions produced by surface states. The relative importance of these two sources of density of states depends strongly on the function $\Delta p(\omega)$ [Eq. (3.14)]. $\Delta p(\omega)$ in turn depends strongly on the surface Madelung potential and the electron occupation of surface orbitals, which must be determined self-consistently.

All of the results described in this section apply to the states derived from the equivalent set $[d_{xz}, p_z(1), p_x(3)]$.

E. $[d_{xy}, p_x(3), p_y(2)]$ Surface states

The remaining set of π orbitals to consider are illustrated schematically in Fig. 5(a). As noted in our previous paper,[4] there is no coupling between orbitals on different layers parallel to the surface. Consequently each layer constitutes a two-dimensional subsystem and the states of each layer are similar to the bulk states. Thus the energy bands are given by

$$E_{xy}(n,K) = \tfrac{1}{2}[E_t(n) + E_\pi(n)] \pm (\{\tfrac{1}{2}[E_t(n) - E_\pi(n)]\}^2 + 4(pd\pi)^2(S_x^2 + S_y^2))^{1/2}. \tag{3.29}$$

The LDS for the cation and anion are given by Eqs. (3.22) and (3.23) using Eq. (3.17) with the replacement

$$\epsilon \to \epsilon(n) = [\omega - \epsilon_t(n)][\omega - \epsilon_\pi(n)] - 4. \tag{3.30}$$

For the model being considered here, $\epsilon(n) = \epsilon$ except for $n = 0$, and when $n = 0$: $\epsilon_t(0) = \epsilon_t + \Delta\epsilon_t$. The quantity $\Delta\epsilon_t$ must be determined self-consistently. In addition, there is a nonbonding state with $\epsilon(n) = \epsilon_\pi(n)$ which produces a δ-function contribution at $\epsilon_\pi(n)$.

F. Summary of the results

We are considering a system possessing nine π bands per unit cell. We found results for the LDS for cations and anions in the surface unit cell associated with each of the nine bands. These results are summarized below.

1. *Nonbonding states*

By adding the various nonbonding contributions one finds that each anion has a LDS due to the nonbonding states

$$\rho_{\alpha,(\mathrm{nb})}(\omega) = \delta(\omega - \epsilon_\pi) \quad (\alpha = z) = 2(2 - 5/\pi)\delta(\omega - \epsilon_\pi), \quad (\alpha = x, y). \tag{3.31}$$

(see Appendix D.)

2. *π and π^* bands: xz and yz*

There are two equivalent contributions from the sets $[d_{xz}, p_x(1), p_z(2)]$ and $[d_{yz}, p_y(1), p_z(3)]$. We found

$$\rho_{\alpha\beta}(\omega) = (-1/\pi)\,|(\omega - \epsilon_\pi)|\,\mathrm{Im}\mathcal{G}(0,0) \quad (\alpha\beta = xz, yz), \tag{3.32}$$

$$\rho_\alpha(\omega) + \rho_\beta(\omega) = (-1/\pi)\,|\omega - \epsilon_t - \Delta\epsilon_t|\,\mathrm{Im}\mathcal{G}(0,0) - (1/\pi)\,|(\omega - \epsilon_\pi)^{-1}|\,[\mathrm{Im}\mathcal{G}(0,0) - (1 + \Delta p)\mathrm{Im}\mathcal{G}(1,0) + \mathrm{Im}\mathcal{G}(2,0)], \quad (\alpha, \beta = x, z \text{ or } y, z). \tag{3.33}$$

3. *π and π^* bands: xy*

For the set $[d_{xy}, p_x(3), p_y(2)]$ we found that

$$\rho_{xy}(\omega) = (-1/\pi)\,|(\omega - \epsilon_\pi)|\,\mathrm{Im}g_{\epsilon'}(0,0), \tag{3.34}$$

with $\epsilon' = (\omega - \epsilon_t - \Delta\epsilon_t)(\omega - \epsilon_\pi) - 4$, and

$$\rho_x(\omega) + \rho_y(\omega) = (-1/\pi)\,|(\omega - \epsilon_t - \Delta\epsilon_t)|\,\mathrm{Im}g_{\epsilon'}(0,0). \tag{3.35}$$

4. *Total LDS*

We can now write expressions for the *total* density of states; for the surface cation LDS (including a factor of 2 for the spin):

$$\rho_{d\pi}(\omega) = (-2/\pi)\,|(\omega - \epsilon_\pi)|\,[2\mathrm{Im}\mathcal{G}(0,0) + \mathrm{Im}g_{\epsilon'}(0,0)], \tag{3.36}$$

with

$$\epsilon = (\omega - \epsilon_t)(\omega - \epsilon_\pi) - 4,$$
$$\epsilon' = (\omega - \epsilon_t - \Delta\epsilon_t)(\omega - \epsilon_\pi) - 4.$$

For the sum of the LDS of the anions in the surface unit cell (including spin)

$$\rho_{p\pi}(\omega) = 2[1 + 2(4 - 10/\pi)]\delta(\omega - \epsilon_\pi) - (2/\pi)\,|\omega - \epsilon_t - \Delta\epsilon_t|\,\mathrm{Im}[2\mathcal{G}(0,0) + g_{\epsilon'}(0,0)] - (4/\pi)\,|(\omega - \epsilon_\pi)^{-1}| \times \mathrm{Im}[\mathcal{G}(2,0) - \mathcal{G}(1,0) - g_\epsilon(2,0) + g_\epsilon(0,0)]. \tag{3.37}$$

These expressions account for a total density of nine bands with two spin states. These bands can accomodate 18 electrons per unit cell.

For the infinite solid the total cation local density of state is

$$\rho_{d\pi}^{\infty}(\omega) = (-6/\pi)\,|(\omega - \epsilon_\pi)|\,\mathrm{Im}g_\epsilon(0,0). \tag{3.38}$$

5. *Special case: $\Delta\epsilon_t = 0$*

For the special case of $\Delta\epsilon_t = 0$ all the Green's functions can be expressed in terms of the complete elliptic integrals of the first kind. We show

in Appendix C that

$$\mathrm{Im}\mathcal{G}(0,0) = \begin{cases} (1/2\pi)(\xi-1)K(|\xi'|) & \text{for } \xi^2 \leq 1, \\ 0 \text{ for } \xi^2 > 1, \end{cases} \tag{3.39}$$

where

$$\xi = \tfrac{1}{4}\epsilon, \quad \xi' = (1-\xi^2)^{1/2}.$$

Therefore, we obtain for the total cation density

$$\rho_{d\pi}(\omega) = (1/\pi^2)\,|\,(\omega-\epsilon_\pi)\,|\,(3-2\xi)K(\xi') \quad \text{with } \xi^2 \leq 1, \tag{3.40}$$

and for the infinite solid:

$$\rho^{\infty}_{d\pi}(\omega) = (3/\pi^2)\,|\,(\omega-\epsilon_\pi)\,|\,K(\xi') \text{ with } \xi^2 \leq 1 \tag{3.41}$$

If it is assumed that the change in the surface Madelung potential vanishes then this solution for $\mathcal{G}(0,0)$ is self-consistent since

$$\int_{-\infty}^{\epsilon_F} d\omega\, \rho_{d\pi}(\omega) = \int_{-\infty}^{\epsilon_F} d\omega\, \rho^{\infty}_{d\pi}(\omega) \quad (\epsilon_\pi < \epsilon_F < \epsilon_t), \tag{3.42}$$

provided ϵ_F, the Fermi energy, lies in the band gap.

6. *Self-consistency condition*

For the model we are considering, the change in the electron occupation of a surface cation due to surface effects on the π states is

$$\Delta n_{d\pi} = 2 \int_{-\infty}^{\epsilon_F} d\omega\, [\rho_{d\pi}(\omega) - \rho^{\infty}_{d\pi}(\omega)], \tag{3.43}$$

where $\rho_{d\pi}(\omega)$ and $\rho^{\infty}_{d\pi}(\omega)$ are given by Eqs. (3.40) and (3.41), respectively.

In addition to changes in n_d due to the π-band LDS, we must also consider how the surface will affect the σ bands, which arise from the e_g and p_σ orbitals. In the examples we are concerned with in this paper, the σ^* bands are unoccupied and changes in LDS in the energy range of the σ^* conduction bands have no effect on Δn_d. However, redistribution of the σ part of the cation LDS in the low-lying σ-valence band could contribute to Δn_d in a significant way. We do not include the effect of the σ bands in this work.

IV. RESULTS AND DISCUSSION

A. LDS of surface ions

We begin by examining the behavior of the LDS as a function of the surface perturbation parameter $\Delta\epsilon_t$ ignoring the self-consistency on the position of the surface state bands on the LDS.

Using the analytic expressions for $g(0,0)$ and $\mathcal{G}(0,0)$ given in Appendices A and B we have calculated the LDS for cations and anions in the surface unit cell. In Fig. 6, we present a series of

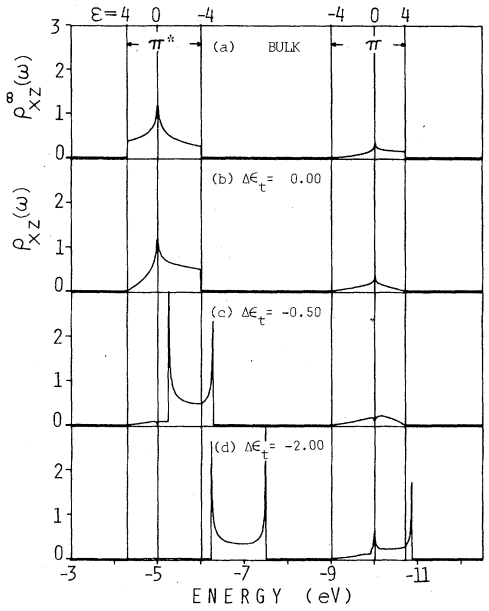

FIG. 6. LDS of a surface cation as a function of the surface perturbation ΔE_t. Only the set $\{d_{xz}, p_x(1), p_z(2)\}$ is considered and $pd\pi = 1.0$ eV. (a) LDS of a cation in the infinite solid; the total density in the π band is 0.555 for each spin, (b) LDS of a surface cation for $\Delta E_t = 0$, (c) $\Delta E_t = -0.5$ and (d) $\Delta E_t = -2.0$ eV. The sets of vertical lines at $\epsilon = \pm 4$ indicate the band edges and those at $\epsilon = 0$ indicate the band centers of the π bands.

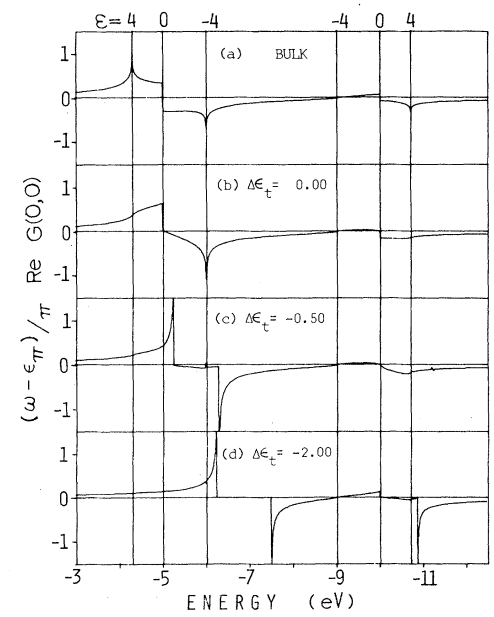

FIG. 7. Real parts of the Green's function $G(0,0)$ weighted by the factor $(\omega-\epsilon_\pi)/\pi$ for the corresponding cases in Fig. 6. $G(0,0)$ represents $\mathcal{G}(0,0)$ in (b) through (d). In (a), $G(0,0)$ represents $g(0,0)$.

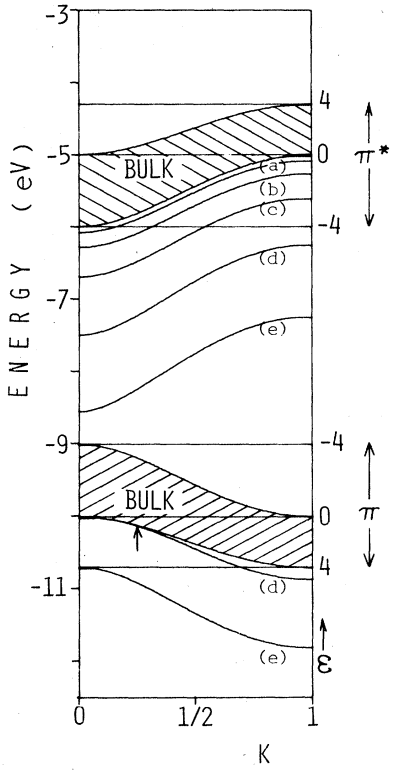

FIG. 8. Surface energy bands of $SrTiO_3$ with parameters $E_t = -6.01$, $E_\pi = -9.02$, and $pd\pi = 1.0$ eV. The labeled curves correspond to different surface perturbations: (a) $\Delta E_t = -0.21$, (b) -0.5, (c) -1.0, (d) -2.0, and (e) -4.0 eV. The vertical arrow on the lower curve (d) indicates the energy and K value where the second surface band merges with the bulk continuum of states.

graphs of the π-band density $\rho^{\infty}_{xz}(\omega)$ and $\rho_{xz}(\omega)$ for different values of $\Delta\epsilon_t$ with $pd\pi = 1$ eV. The real parts of $g(0,0)$ and $\mathcal{G}(0,0)$ are shown in Fig. 7 for the corresponding cases. In Fig. 6(a), we show the bulk density of states $\rho^{\infty}_{xz}(\omega)$. The vertical lines at $\epsilon = \pm 4$ designate the band edges of the π and π^* bands and the vertical lines at $\epsilon = 0$ designate the corresponding band centers. Figure 6(b) shows the surface cation LDS for the "perfect" surface for which there are no surface perturbations, i.e., $\Delta\epsilon_t = 0$. For this case there are no surface states, however, there is a substantial redistribution of the density due to the existence of the surface. It can be seen that the density is depleted from the top of the π^* band and increased at the bottom of this band. The enhancement of density near the bottom of the π^* band is a precurser to the emergence of surface states in the band gap. Figure 6(c) illustrates the LDS with $\Delta\epsilon_t = -0.5$ for which a surface band exists in the band gap below the π^*-band edge. It appears that the surface band states overlap the bulk states, however the surface states always have a lower energy than the corresponding bulk state having the same wave vector. This is apparent in Fig. 8, which shows the dispersion curves as a function of the wave vector. If we increase the surface perturbation to $\Delta\epsilon_t = -2.0$, shown in Fig. 6(d), the surface band moves completely into the band-gap region. The LDS in the π^*-band range is very nearly zero and all of the density lies in the surface band. This indicates that the surface ions no longer participate in the bulklike states of the semi-infinite solid. In the same figure, one also sees a second surface band emerging partially from the bottom of the valence band, however, Fig. 8(d) shows that this new surface band is truncated at one side (indicated by an arrow) by the bulk band. The occurrence of this second surface band below the π band has important implications with regard to the self-consistency conditions. The states involved in this band will be occupied with electrons even when the Fer-

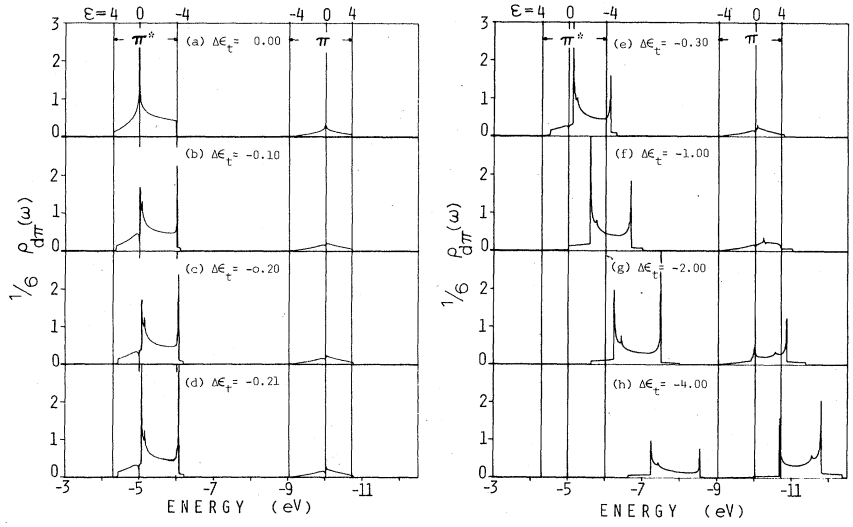

FIG. 9. Total LDS functions given by Eq. (3.36) for different surface perturbations: (a) $\Delta E_t = 0$, (b) -0.1, (c) -0.2, (d) -0.21, (e) -0.3, (f) -1.0, (g) -2.0, and (h) -4.0 eV, where the vertical lines indicate the band edges and band centers, and $pd\pi = 1.0$ eV. The integral of the density in and below the π band is (a) 0.498; (b) 0.498; (c) 0.501; (d) 0.504; (e) 0.522; (f) 0.681; (g) 1.062; and (h) 1.950 for each spin.

mi level is below the band-gap surface states. We shall return to this point in Sec. IV B where we discuss the effects of self-consistency.

In Fig. 9, we present a series of graphs of the surface cation LDS $\rho_{d\pi}$ (which includes all of the π-band contributions) for $\Delta\epsilon_t$ varying from 0 to −4. In all of the examples presented $pd\pi = 1$ eV. The structure in $\rho_{d\pi}$ is easily understood in terms of the different types of Van Hove singularities. The surface bands associated with d_{xz} (or d_{yz}) orbitals produce square root singularities characteristic of a one-dimensional band. The contributions of states derived form d_{xy} orbitals have characteristic two-dimensional structure; jump discontinuities at the band edges and a logarithmic singularity at the band center. Thus, for example, in Fig. 9(g) one sees two square-root singularities at $E \approx -7.5$ and −6.2 eV from the band-gap surface band and a third square-root singularity at $E \approx -10.9$ eV due to the partial surface band below the π band. The peaks at $E \approx -6.3$ and −10.5 eV are logarithmic singularities and the jump discontinuities are evident at $E \approx -5.6$, −8.0, and −11.4 eV.

It is clear from Fig. 9 that as $\Delta\epsilon_t$ becomes more negative there is a substantial increase in the cation LDS in the valence-band region. For example, in Fig. 9(h), $\rho_{d\pi}$ has more density below the π band than above it.

Figure 10 illustrates the behavior of $\rho_{d\pi}$ for positive values of $\Delta\epsilon_t$. It is seen that there is an increasing depletion of density in the valence band regime as surface state bands are formed above the π^* band.

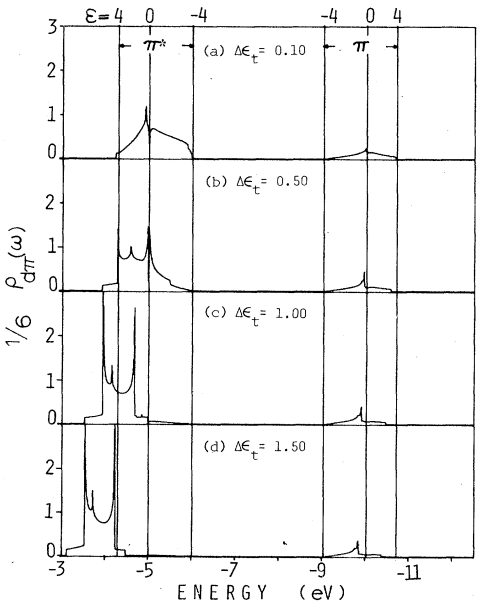

FIG. 10. Total LDS functions with surface perturbations ΔE_t positive: (a) $\Delta E_t = 0.1$, (b) 0.5, (c) 1.0, and (d) 1.5 eV. $pd\pi$ is taken to be 1.0 eV. The integral of the density in and below the π band is (a) 0.447; (b) 0.408; (c) 0.354; and (d) 0.306 for each spin.

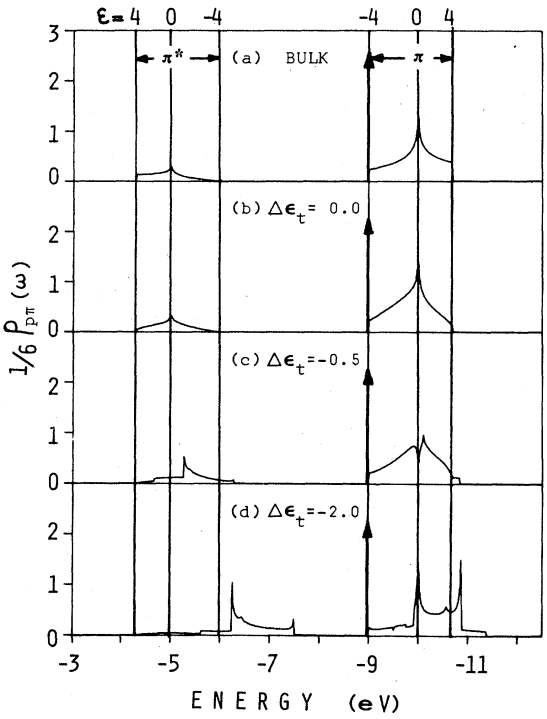

FIG. 11. Total LDS functions given by Eq. (3.23) for a bulk anion (a) and Eq. (3.37) for a surface anion with (b) $\Delta E_t = 0$, (c) −0.5, and (d) −2.0 eV. The arrows at $E = E_\pi = -9.02$ eV correspond to the peaks due to the δ-function contributions which contain 3 states/spin for the bulk anion and 2.63 states/spin for the surface anion. The integral of the density in and below the π band is (a) 2.45; (b) 2.78; (c)2.52; (d) 2.38 for each spin.

In Fig. 11, the sum of the LDS for the oxygen anions in the surface unit cell, $\rho_{p\pi}(\omega)$ is presented for various values of $\Delta\epsilon_t$. In comparing Fig. 11 with Fig. 9 it is clearly seen that the states are admixtures of p and d orbitals. The arrows in Fig. 11 indicate the position of the π^0 nonbonding state, which contributes a δ function contribution to the density of states of the anions.

B. Self-consistent results

In this section we address the question of treating the change in the electron occupancy of d orbitals in an approximate self-consistent manner. In Sec. III B we expressed the surface perturbation parameter $\Delta\epsilon_t$ in terms of two contributions according to the relation

$$\Delta\epsilon_t = -\Delta V_M^0 + (U_d - C_M)\Delta n_d(0)\,. \tag{4.1}$$

The quantity $-\Delta V_M^0$ is the reduction of the repulsive

Madelung potential at a surface cation site with the occupation of the p and d orbitals equal to their bulk values. The second term represents approximately the change in the Coulomb repulsion energy among d electrons and the change in the surface cation Madelung potential due to changes in the electron occupation of ions in the surface unit cell. If $\Delta n_d(0)$ is positive, charge is transferred from anions to surface cations. This changes the effective valence state of the surface cation. Consider, for example, a free Ti^{3+} ion. The ionization energy for liberating a d electron to produce Ti^{4+} is 43 eV while the ionization energy for $Ti^{2+} \rightarrow Ti^{3+}$ is only 24 eV. This suggests that for the free ion U_d for the repulsion among d electrons on a Ti cation is about 19 eV. The value for an ion in the solid is of course expected to be much smaller because of polarization and screening effects.

For $\Delta n_d(0)$ positive, the charge on the anions in the surface unit cell will be reduced. This will reduce the effective repulsive Madelung potential seen by the cation. We may estimate C_M of Eq. (4.1) by considering the change in the Madelung potential at a surface cation site due to changing the charges of the surface unit cell. This is easily calculated from the tables given in our previous paper on the Madelung potentials of perovskites.[9] Assuming the B-ion charge is changed by $\Delta n_d(0)$ and the surface oxygen ion charge is changed by $\frac{1}{2}\Delta n_d(0)$ gives $C_M \simeq 10$ eV. Other assumptions about the redistribution of charge produce comparable estimates for C_M provided the changes are localized in the surface unit cell. This estimate of C_M is based on a point ion model for nonpolarizable ions. One expects that C_M is reduced in the solid in a manner analogous to the reduction of U_d.

The difference $U_d - C_M$ for bare ions is of the order of 8 eV. The appropriate value for the solid is not known. We assume that polarization and screening reduce this difference to about 4 eV. The qualitative results which we discuss in what follows do not depend sensitively on the precise value of $U_d - C_M$ but only upon the assumption that U_d is larger than C_M.

Now consider Fig. 9(g) with $\Delta\epsilon_t = -2$. This case is approximately what we expect for $SrTiO_3$ ignoring changes in the surface ion charges. The bulk LDS for a cation is shown in Fig. 6(a). If the crystal is insulating with the Fermi level at midgap then only the density below midgap corresponds to filled states. For the cation in the interior the number of electron in filled states associated with t_{2g} d orbitals [Fig. 6(a)] is 1.1. The number of electrons in filled states for a surface ion with the LDS of Fig. 9(g) is 2.1. Therefore an additional electron could reside on each surface cation even though the band-gap surface states are unoccupied. As a result Coulomb repulsion is substantial even when the band-gap states are empty. The origin of this effect is an increased covalent mixing of d orbitals into the filled valence band states of the finite solid. We refer to this effect as "surface enhanced covalency." The additional electrons in d orbitals would come from the anions. For example, there are 10.9 electrons occupying the anion orbitals of the π bands for the bulk sample [Fig. 11(a)] while for $\Delta\epsilon_t = -2$ [Fig. 11(d)] there are only 10 electrons in these bands.

The presence of an extra electron in surface d orbitals results for $\Delta\epsilon_t = -\Delta V_M^0 = -2$ eV. This is not a self-consistent solution. The calculated value of $\Delta\epsilon_t$ using Eq. (4.1) and $\Delta n_d(0) = 1$ is $\Delta\epsilon_t = +2$ assuming the Fermi level to be at midgap. By varying $\Delta\epsilon_t$ with $-\Delta V_M^0$ at -2 eV one finds a self-consistent solution for $\Delta\epsilon_t = -1.0$, $\Delta n_d(0) = 0.25$, and $U_d - C_M = 4$ eV. This solution is illustrated in Fig. 9(f). Comparing the non-self-consistent solution Fig. 9(g) with Fig. 9(f) it is seen that the effect of Coulomb repulsion is to force the surface band out of the band gap toward the conduction-band edge.

Next, we consider the case of a doped or reduced sample for which the Fermi level is at the bottom of the π^*-band edge. Neglecting Coulomb repulsion the band-gap states of Fig. 9(f) would be filled. The self-consistent solution is illustrated by Fig. 9(d) with $\Delta\epsilon_t = -0.21$ and $\Delta n_d(0) \simeq 0.446$ for $U_d - C_M = 4$ eV. It is evident that the surface band has been effective expelled from the band gap. The peak in the surface-state density is only about 0.1 eV into the band-gap region.

If the σ bands involving the e_g d orbitals are also included the surface enhanced covalency effect is further increased. This would have the same effect as increasing the parameter $U_d - C_M$. Therefore, it seems possible that the surface-state bands may be forced to lie very near to the Fermi level.

This suggests that the Fermi level is not "pinned" by the surface states as is usually assumed for simple semiconductors. Indeed, it appears that the converse is more nearly true; the Fermi level, in effect, pins the surface states.

C. Discussion

According to the results described in Sec. IV B, attempts to fill the one-electron surface states result in the expulsion of the states from the band gap region. This effect offers a plausible explanation of the absence of band gap states on reduced or doped samples of $SrTiO_3$ and TiO_2 as reported by Powell and Spicer[12] and by Henrich *et al.*[13]

For the insulating state (Fermi level at midgap) surface bands may exist deeper in the band gap than for the reduced state (Fermi level near the

conduction-band edge). It may be possible to locate the position of band gap states for insulating $SrTiO_3$ or TiO_2 if optical,[17] photoemission,[18] or electron-energy-loss experiments capable of detecting empty final states could be performed.

Our model also suggests that the valence-band LDS of both cations and anions is strongly dependent on the position of the band-gap surface states. Thus one would expect the valence-band structure to change substantially in photoemission or electron-energy-loss experiments as the sample is changed from an insulator to the highly reduced state. Further calculations including the σ bands are needed in order to be able to utilize this effect in a quantitative manner.

The results of our model are strongly dependent on the shift in the diagonal energy $\Delta\epsilon_t$ and therefore upon the relative of importance of intra-atomic Coulomb repulsion compared with the interatomic Madelung potentials. In the examples presented here the Coulomb repulsion among excess electrons on cation sites is dominant. This seems to be a reasonable assumption since otherwise the compound could not possess ionic character.

On the other hand, surface reconstruction or the presence of surface vacancies can substantially alter the balance between intra and interatomic Coulomb effects. A surface oxygen vacancy will contribute an attractive term to the Madelung potential of first-, second-, and third-nearest-neighbor surface cations of $(e/a)\,q_{\rm eff}$, $(e/(5)^{1/2}a)\,q_{\rm eff}$, and $(e/3)\,q_{\rm eff}$, respectively, where $q_{\rm eff}$ is the effective charge on the oxygen ions and a is the cation-anion distance. Even with $q_{\rm eff}=1$, $(e/a)\,q_{\rm eff}=7.4$ eV, $(e/(5)^{1/2}a)\,q_{\rm eff}=3.3$ eV and $(e/3a)\,q_{\rm eff}=2.5$ eV. The existence of surface vacancies in the concentrations of 3% or 4% of the oxygen per surface unit cell would be sufficient to compensate intra-atomic Coulomb repulsion and stabilize the occurrence of surface states in the band gap similar to those of Fig. 9(g) with excess electrons in surface d orbitals for charge neutrality.

Surface states in the band gap of $SrTiO_3$ and TiO_2 have been observed by Henrich *et al.*[13] when the sample surface has been chemically processed or subjected to Ar^+-ion bombardment. It is believed that such surfaces, although well ordered as evidenced by LEED patterns, have a higher-surface oxygen vacancy concentration than vacuum cleaved or fractured surfaces.

In their study of TiO_2, Henrich *et al.* indicate that three regions occur as a function of increasing Ar^+-ion bombardment. Region I corresponds to small concentrations of oxygen vacancies. They suggested that at the higher concentrations in regions II and III the surface gradually becomes reconstructed from one characteristic of TiO_2 to one characteristic of Ti_2O_3. Our band theory results should apply qualitatively to region I, but not to regions II and III.

The model explains most of the experimentally observed results cited in the introduction if it is assumed that cut and chemically processed surfaces of $SrTiO_3$ or ion-bombarded surfaces of $SrTiO_3$ and TiO_2 have an abundance of surface oxygen vacancies, while vacuum-fractured surfaces do not. This leaves unexplained the absence of band-gap surface states on chemically prepared TiO_2 samples. We may only speculate that the chemical effect of etching on $SrTiO_3$ differs from that of TiO_2 because of the difference in crystal structures. The model also does not explain the poor LEED patterns observed on vacuum fractured surfaces, but does assume that the origin of the apparent disorder is not oxygen vacancies.

In conducting materials such as Ti_2O_3, the intra-atomic Coulomb integral U_d is likely to be much smaller because the energy difference between relevant Ti-ion ionization states is smaller and also because there are ample conduction electrons to provide screening. The concept of point ion Madelung potentials is also inapplicable. However, the basic idea that the increase in intra-atomic Coulomb energy is opposed to the corresponding decrease in interatomic Coulomb energy remains valid. A more careful study of this problem is required in order to arrive at qualitative conclusion. However, it would not be surprising if band-gap surface states were stable in Ti_2O_3 without oxygen vacancies.

It is emphasized that even though the self-consistent surface-state solutions are forced to lie near to the conduction band edge they nevertheless are still highly localized and possess the same symmetry properties as a surface band lying deeper in the band gap. Consequently, one may expect that these surface states will be of importance in the surface chemistry of the oxides as previously suggested.[8,11]

ACKNOWLEDGMENTS

This research was supported in part by the NSF. Acknowledgement is made to the Donors of the Petroleum Research Fund, administered by the American Chemical Society, for the partial support of this work.

APPENDIX A: EVALUATION OF $g_\epsilon(0,0)$

The infinite-bulk Green's function for $n=n'=0$ and $l=l'$ is given from Eq. (3.13) by

$$g_\epsilon(0,0)=\frac{1}{\pi}\int_0^\pi \frac{dK}{2i\sin\theta}\,, \tag{A1}$$

where $\theta(\omega,K)$ and ϵ are defined in Eqs. (3.16) and (3.17), respectively, as

$$-2\cos\theta = 2\cos K + \epsilon \tag{A2}$$

and

$$\epsilon = (\omega - \epsilon_\pi)(\omega - \epsilon_t) - 4 . \tag{A3}$$

If we call $t \equiv -\cos\theta = \cos K + \frac{1}{2}\epsilon$, then Eq. (A1) takes the form

$$g_\epsilon(0,0) = -\frac{1}{2\pi}\int_{\epsilon/2+1}^{\epsilon/2-1} dt\,[(t-1)(t+1)(1+\tfrac{1}{2}\epsilon - t) \times (1-\tfrac{1}{2}\epsilon + t)]^{-1/2}, \tag{A4}$$

which can be expressed in terms of the complete elliptic functions of the first kind.[19] For different values of ϵ one finds:

$$g_\epsilon(0,0) = (1/2\pi)\,\xi^{-1}K(\xi^{-1}) \quad \text{for } |\epsilon| > 4 , \tag{A5}$$

$$g_\epsilon(0,0) = (1/2\pi)\,[\mathrm{sgn}(\xi)K(\xi) - iK'(\xi)] \quad \text{for } |\epsilon| < 4 , \tag{A6}$$

where

$$\xi^2 = (\tfrac{1}{4}\epsilon)^2 , \quad K'(\xi) = K(\xi') = K((1-\xi^2)^{1/2}) .$$

We note that when the real part of $g_\epsilon(0,0)$ has a jump discontinuity at an energy ω_i, then the imaginary part of $g_\epsilon(0,0)$ has a logarithmic singularity at that energy ω_i, and vice versa. Moreover, both the real and the imaginary parts of $g_\epsilon(0,0)$ are symmetric with respect to the midgap, i.e., $\omega_0 = \frac{1}{2}(\epsilon_t + \epsilon_\pi)$. The above are also true for $g(0,0)$ when $\Delta\epsilon_t = 0$, but if $\Delta\epsilon_t \neq 0$ then the surface states are produced and the symmetry is broken. In the calculation of the LDS for infinite bulk and perfect surface with $\Delta\epsilon_t = 0$ we lose the symmetry because of the factor $(\omega - \epsilon_\pi)$ which causes the density to vanish at the top of the valence π band.

APPENDIX B: EVALUATION OF $g(0,0)$

Setting $n = n' = 0$ and $l = l' = 0$ in Eq. (3.12), we obtain

$$g(0,0) = \frac{1}{\pi}\int_0^\pi \frac{dK}{\Delta p - e^{-i\theta}} , \tag{B1}$$

with the condition that $\theta(\omega,K)$ changes sign when $\cos\theta < -1$, where $\Delta p(\omega)$ and $\theta(\omega,K)$ are defined in Eqs. (3.14) and (3.15), respectively. Multiplying the numerator and the denominator of the integrand in Eq. (B1) by $(\Delta p - e^{i\theta})$, we can separate $g(0,0)$ into two terms as:

$$g(0,0) = G_1 \pm G_2 , \tag{B2}$$

where

$$G_1 = \frac{1}{2\Delta p}\left[1 - \frac{i}{\pi}\int_{-1}^{1}\left(\frac{1-(x+\frac{1}{2}\epsilon)^2}{1-x^2}\right)^{1/2}\frac{dx}{\Omega + x}\right], \tag{B3}$$

and

$$G_2 = \frac{1}{2\Delta p}\left(\frac{\Delta p^2 - 1}{2\Delta p}\right)\frac{1}{\pi}\int_{-1}^{1}\frac{dx}{\Omega + x} . \tag{B4}$$

The minus sign in front of G_2 is used when $\Omega < -1$, where the substitution of $x = \cos K$ is made in obtaining Eq. (B2) from (B1) and Ω is defined in Eq. (3.28).

G_2 can be solved easily in terms of Ω and Δp and given by

$$G_2 = \frac{1}{2\Delta p}[(\Delta p^2 - 1)/2\Delta p](\Omega^2 - 1)^{-1/2} , \tag{B5}$$

and using standard tables,[19] G_1 can be evaluated in terms of the complete elliptic integrals of the third kind as

$$G_1 = (1/2\Delta p)\{1 + (2/\pi)(1+\xi)[\alpha\Pi(-\beta\xi, |\xi|) - \Pi(-\xi, |\xi|)]\}, \quad \text{for } |\epsilon| > 4, \tag{B6a}$$

and

$$G_1 = [(1+\eta)/\pi\Delta p]\,\mathrm{sgn}(\epsilon)[\alpha\Pi(-\beta\eta, |\eta|) - \Pi(-\eta, |\eta|)] + \mathrm{sgn}(\gamma)G_2 - (i\eta/\pi\Delta p)[\beta\Pi(\alpha(1+\eta), |\eta'|) - \Pi(1+\eta, |\eta'|)], \quad \text{for } |\epsilon| < 4 , \tag{B6b}$$

with

$$\alpha = (\Delta p + 1)^2/(\Omega + 1) , \quad \beta = (\Delta p - 1)^2/(\Omega + 1) , \quad \gamma = (\Delta p^2 - 1)/\Delta p , \quad \eta' = 1 - \eta^2 , \quad \eta = \xi^{-1} = \tfrac{1}{4}\epsilon , \tag{B7}$$

where

$$\Pi(\alpha^2, k) = \int_0^{\pi/2}\frac{d\theta}{(1-\alpha^2\sin^2\theta)(1-k^2\sin^2\theta)^{1/2}} . \tag{B8}$$

When surface bands are formed, both G_1 and G_2 have square-root Van Hove singularities in their real and imaginary parts at the surface state band edges. The density corresponding to the bulklike states of the finite solid arises from branch-cut contributions to G_1.

APPENDIX C: SPECIAL CASE: $\Delta p = 1$

For the special case $\Delta\epsilon_t = 0$, from Eq. (3.14), we have

$$\Delta p = 1 . \tag{C1}$$

Then, from Eq. (3.12) or (B1), we get

$$g_0(0,0)=\frac{1}{\pi}\int_0^{\pi}\frac{dK}{1-e^{-i\theta}} \tag{C2}$$

or

$$g_0(0,0)=\frac{1}{2}\left[1-\frac{i}{\pi}\int_{-1}^{1}dx\left(\frac{1-\frac{1}{2}\epsilon-x}{(1+\frac{1}{2}\epsilon+x)(1-x^2)}\right)^{1/2}\right]. \tag{C3}$$

Similarly, we get

$$g_0(0,0)=\tfrac{1}{4}-(1/2\pi)(1-\xi^{-1})K(|\xi^{-1}|) \quad \text{for } |\epsilon|>4, \tag{C4}$$

$$g_0(0,0)=\tfrac{1}{4}+(1/2\pi)(1-\xi)[\mathrm{sgn}(\xi)K(|\xi|)-iK'(|\xi|)] \quad \text{for } |\epsilon|<4, \tag{C5}$$

where $\xi=\frac{1}{4}\epsilon$,

$$K'(|\xi|)=K((1-\xi^2)^{1/2}).$$

The same result can be obtained by taking the limits of the results in Appendix B as Δp approaches unity.

APPENDIX D: OTHER USEFUL GREEN'S FUNCTIONS

In the evaluation of p-orbital LDS functions at a surface anion and p- and d-orbital LDS functions at inner layers one needs to utilize the function

$$F_n(\omega)=g(2n,0)-g_\epsilon(2n,0)+g_\epsilon(0,0), \tag{D1}$$

as in Eqs. (3.11) and (3.37). Equation (D1) can be expressed in terms of lower-order Green's functions $g(m,l)$ and $g_\epsilon(m,l)$ with the help of two recurrence relations:

$$\Delta p\, g(m,l)=g(m-1,l)+I(m,l), \tag{D2}$$

and

$$I(m,l)=g_\epsilon(m+1,l)-g_\epsilon(m-1,l), \tag{D3}$$

where $g(m,l)$ and $g_\epsilon(m,l)$ are defined in Eqs. (3.12)–(3.17) and

$$I(m,l)=\frac{1}{\pi}\int_0^{\pi}e^{im\theta}e^{ilK}dK. \tag{D4}$$

Exact, analytical expressions for $g(0,0)$ and $g_\epsilon(0,0)$ are given in Appendices A–C, hence in order to calculate $g(m,0)$ and $g_\epsilon(m,0)$ one only needs the solutions for $I(m,0)$. In what follows we will present the exact solutions for $I(m,0)$ with $m=1$ and 2 which are needed for the p-orbital surface states:

$$I(1,0)=\begin{cases}-\frac{1}{4}\epsilon[1-(2/\pi)E(k)], & k=4/|\epsilon|,\\ -\frac{1}{4}\epsilon+(2/\pi)\{\mathrm{sgn}(\epsilon)[E(k)-k'^2K(k)]+i[E'(k)-k^2K'(k)]\}, & k=\frac{1}{4}|\epsilon|,\end{cases} \tag{D5}$$

and

$$I(2,0)=\begin{cases}\frac{1}{4}\epsilon^2\{[1-(2/\pi)E(k)]-(1/\pi[E(k)-k'^2K(k)]\}, & k=4/|\epsilon|,\\ \epsilon(\frac{1}{4}\epsilon-(2/\pi)\,\mathrm{sgn}(\epsilon)\{\frac{1}{2}E(k)+[E(k)-k'^2K(k)]\}+(2/\pi)i\{\frac{1}{2}[K'(k)-E'(k)]-[E'(k)-k'^2K'(k)]\}), & k=\frac{1}{4}|\epsilon|,\end{cases} \tag{D6}$$

where $\epsilon(\omega)$ is given by Eq. (3.17). Thus the LDS function for the p electrons on an anion site at the surface is given, from Eq. (3.21), by $-1/\pi$ times the imaginary part of the Green's function

$$G_p(0)=(\omega-\epsilon_t-\Delta\epsilon_t)g(0,0)+(\omega-\epsilon_\pi)^{-1}[1+F_2(\omega)-g(1,0)], \tag{D7}$$

or

$$G_p(0)=(\omega-\epsilon_t-\Delta\epsilon_t)g(0,0)+(\omega-\epsilon_\pi)^{-1}\{1-I(1,0)+(1/\Delta p)I(2,0)+[(1-\Delta p)/\Delta p^2][g(0,0)+I(1,0)]\}, \tag{D8}$$

where we made the use of Eqs. (3.21) and (D1)–(D3).

Within the approximation we have assumed to begin with that the oxygen-oxygen interactions ($pp\pi$) negligible with respect to the transition metal-oxygen interactions ($pd\pi$); the nonbonding bands are flat and the LDS for them are just δ functions at $\omega=\epsilon_\pi$ with strengths being equal to one for the x-y-plane solution (parallel to the surface) and to the real part of the second term in Eq. (D8) at $\omega=\epsilon_\pi$ for each of the x-z- and y-z-plane solutions:

$$C_\alpha=\begin{cases}1, & \text{for } \alpha=xy,\\ \mathrm{Re}\{1-I(1,0)+(1/\Delta p)I(2,0)+[(1-\Delta p)/\Delta p^2][g(0,0)+I(1,0)]\}|_{\omega=\epsilon_\pi}, & \text{for } \alpha=xz \text{ or } yz.\end{cases} \tag{D9}$$

This can be calculated easily, since $\Delta p = 1$ at $\omega = \epsilon_\pi$ from Eq. (3.14) and $\epsilon = -4$ at $\omega = \epsilon_\pi$ from Eq. (3.17); therefore, Eq. (D9) gives for $\alpha = x, z$ or y, z,

$$C_\alpha = \mathrm{Re}[1 - I(1,0) + I(2,0)]\,|_{\epsilon=-4}$$

and (D10)

$$= 1 + (4 - 12/\pi) - (1 - 2/\pi) = 2(2 - 5/\pi)\,,$$

thus, the total strength of the δ function which describes the nonbonding LDS in this model is

$$\sum_\alpha C_\alpha = 1 + 4(2 - 5/\pi) = 9 - 20/\pi \cong 2.634\,. \quad \text{(D11)}$$

With the present knowledge one can also calculate the LDS function for a d electron on a cation site at the layer next to the surface into the bulk using Eqs. (3.3), (3.11), and (D1)–(D3) as

$$\rho_{d\pi}^{(1)}(\omega) = -(1/\pi)\,\mathrm{Im}G_{xz}(1,0;1,0) = -(1/\pi)(\omega - \epsilon_\pi)\,\mathrm{Im}F_2(\omega)\,, \quad \text{(D12)}$$

with

$$F_2(\omega) = (1/\Delta p^2)[\vartheta(0,0) + I(2,0)] + [(1 - \Delta p)/\Delta p]I(1,0)\,, \quad \text{(D13)}$$

where $\vartheta(0,0)$, $I(1,0)$, $I(2,0)$, and Δp are given by Eqs. (B6a) and (B6b), (D5), (D6), and (3.14), respectively.

---

*On leave from Middle East Technical University, Ankara, Turkey.

[1]P. E. Emmet, P. Sabatier, and E. E. Reid, *Catalysis Then and Now* (Franklin, Philadelphia, 1965).
[2]A. Fujishima and K. Honda, Nature 238, 37 (1972).
[3]J. G. Mavroides, D. I. Tchernev, J. A. Katalas, and D. F. Kolesar, Mat. Res. Bull. 10, 1023 (1975).
[4]T. Wolfram, E. A. Kraut, and F. J. Morin, Phys. Rev. B 7, 1677 (1973).
[5]T. Wolfram, Phys. Rev. Lett. 29, 1383 (1972), where Eq. (2) should read

$$G(E) = (\xi/\pi)\,|E - \tfrac{1}{2}(E_t + E_\perp)|\,K(\xi)/(pd\pi)^2,$$

with

$$\xi = \frac{4}{\zeta} \text{ and } \zeta = \frac{(E - E_t)(E - E_\perp) - 4(pd\pi)^2}{(pd\pi)^2}$$

[6]L. F. Mattheiss, Phys. Rev. B 6, 4718 (1972).
[7]M. Cardona, Phys. Rev. 140, A651 (1965).
[8]F. J. Morin and T. Wolfram, Phys. Rev. Lett. 30, 1214 (1973).
[9]E. A. Kraut, T. Wolfram, and W. F. Hall, Phys. Rev. B 6, 1499 (1972).
[10]T. Wolfram, R. Hurst, and F. J. Morin, Phys. Rev. B (to be published).
[11]T. Wolfram and F. J. Morin, Appl. Phys. 8, 125 (1975); T. Wolfram, F. J. Morin, and R. Hurst, in Electrocatalysis on Non-Metallic Surfaces, Natl. Bur. Stds. Spec. Publ. (U.S. GPO, Washington, D. C., to be published).
[12]R. A. Powell and W. E. Spicer, Phys. Rev. B 13, 2601 (1976).
[13]V. E Henrich, G. Dresselhaus, and H. J. Zeiger, Phys. Rev. Lett. 36, 1335 (1976); in Ref. 11; Solid State Research Report, Lincoln Laboratory, M.I.T. (1976:2) (unpublished).
[14]J. B. Goodenough, Prog. Solid State Chem. 5, 145 (1971).
[15]J. C. Slater and G. F. Koster, Phys. Rev. 94, 1498 (1954).
[16]D. N. Zubarev, Ups. Fiz. Nauk 71, 71 (1960) [Sov. Phys. Ups. 3, 320 (1960)].
[17]G. Chiarotti, S. Nannarone, R. Pastore, and P. Chilaradia, Phys. Rev. B 4, 3398 (1971).
[18]D. E. Eastman and J. L. Freeouf, Phys. Rev. Lett. 33, 1601 (1974).
[19]P. F. Byrd and M. D. Friedman, *Handbook of Elliptic Integrals for Engineers and Scientists* (Springer-Verlag, Berlin, 1971), 2nd ed., revised.